Nanoscale

RSCPublishing

ARTICLE

Engineering the synthesis of silica-gold nano-urchin particles using continuous synthesis

Cite this: DOI: 10.1039/x0xx00000x

Víctor Sebastián,[a,b‡,] Seung-Kon Lee [a,c‡] and Klavs F. Jensen[a*]

Received 00th January 2012,
Accepted 00th January 2012

DOI: 10.1039/x0xx00000x

www.rsc.org/

Compared to freestanding nanoparticles, supported nanostructures typically show better mechanical stability as well as ease of handling. Unique shapes such as core-shells, raspberries and crescents have been developed on supported materials to gain improved chemical and optical properties along with versatility and tunability. We report the formation of hyper-branched gold structures on silica particles, silica-gold nano-urchin (SGNU) particles. Kinetic control of crystallization, fast mass transfer as well as a bumped surface morphology of the silica particles are important factors for the growth of gold branches on the silica support. Using a microfluidic platform, continuous synthesis of SGNUs is achieved with increased reaction rate (less than 12 min. of residence time), better controllability and reproducibility than that obtained in batch synthesis. The hyper-branched gold structures display surface-enhanced Raman scattering (SERS).

Introduction.

Microfluidic systems offer excellent conditions for synthesis of nanomaterials by control of mixing, temperature, and pressure combined with fast heat and mass transfer.[1, 2] Moreover, they enable controlled synthesis under higher temperature and pressure conditions than typically feasible in batch with resulting faster synthesis.[1, 3] Herein, we report batch and microfluidic synthesis of hyper-branched gold structures on silica particles, silica-gold nano-urchin (SGNU) particles. The formed particles consist of a dielectric silica core decorated with densely packed gold nanobranches stretching outward. The morphology serves as an active substrate for tip-enhanced Raman scattering,[4] and could additional have applications in catalysis and bio-imaging.[5, 6]

Gold nanoparticles have been synthesized by a variety of approaches for diverse applications in catalysis, bio-imaging, drug delivery and photovoltaics. Their surface plasmon resonance (SPR) and surface enhanced Raman scattering (SERS) properties have been of particular interest for photothermal therapy and molecular sensing, respectively[7-15]. SERS active structures have been fabricated by complex with top-down methods,[4, 12, 16, 17] but wet-chemical synthesis of gold nanoparticles offer potential advantages in simple, high yield, and limited scalable synthesis.[12, 18, 19, 20, 21,22]

Gold nanostructures, such as nanorods, nanowires, tetrapods, nanoplates and star-shaped particles are particularly attractive for many applications because of their strong confinement of the electromagnetic field and high enhancement that can be tuned over a wide range of optical wave lengths in comparison with ordinary spherical structures.[11, 23-27] Combination of the metal nanostructure with a support material, such as in core-shells, raspberries, and crescents, affords additional advantages in tuning optical properties, improved chemical/mechanical stability, and ease of handling compared to free-standing nanoparticles.

Batch methods,[20] specialized ligands[28] and additional electrochemical treatments[29] have typically been needed to synthesize these optical architectures, but create challenges in achieving desired optical properties and sufficient reproducibility. Herein we develop a method based on molecular self-assembly and reduction chemistry of gold species to grow gold nanobranches on the surface of silica nanoparticles. The surface roughness of the silica nanoparticle substrates together with kinetic parameters and reagent addition become determining factors in promoting urchin-like growth of the gold structures. We next demonstrated that continuous microfluidic synthesis of the SGNUs provided better control and reproducibility through manipulation of the reagent ratio and enhanced mixing. Finally, the synthesized SGNUs are shown to exhibit significant enhancement of SERS signals from their unique urchin-like morphology with abundant sharp tips.

Results and Discussion

Synthesis of SGNU and characterization

The synthesis procedure of the SGNU particles is based on the common route of gold nanoshells formation as shown in **Fig. 1a**.[30] The procedure involves the synthesis of dielectric core materials, typically silica or polystyrene and their surface

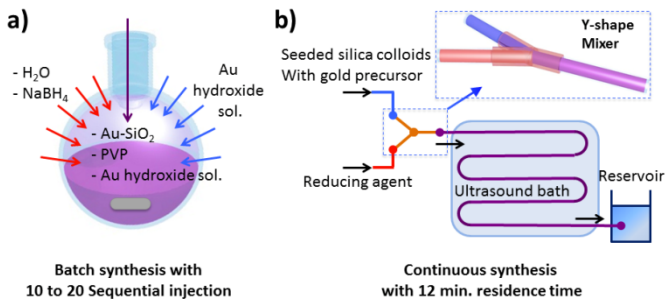

Figure 1.Synthesis procedures to produce SGNU nanoparticles. a) Batch production with sequential addition of reagents. Gold hydroxide solution and $NaBH_4$ solutions were added under a 2 minutes frequency. b) Microfluidic approach injecting the reagents in continuous mode. The residence time was kept constant at 12 minutes.

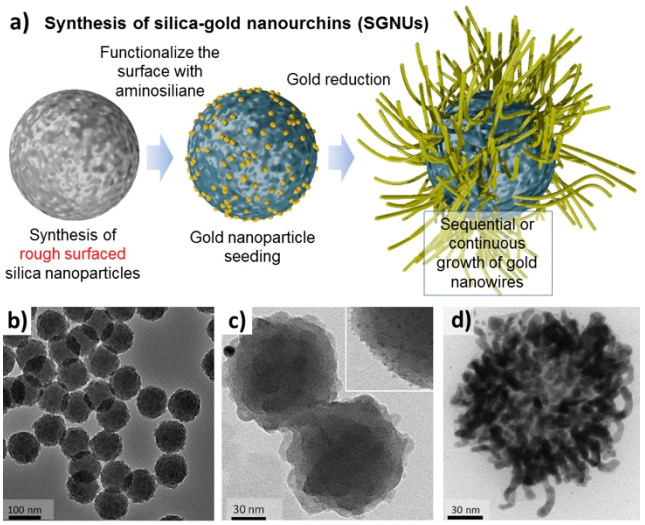

Figure 2. Scheme for the synthesis of silica-gold nanourchins (SGNUs) with representative TEM images of each step. a) Scheme for the synthesis of SGNUs by seeded growth of gold nanobranches on a rough silica nanoparticle surface. b–d) corresponding TEM images at each step. b) TEM images of monodispersed silica nanoparticles with roughened surface feature. c) TEM images of gold seeded silica nanoparticles. Inset shows magnified image of the gold seeds on the silica surface. d) TEM image of synthesized SGNU particles via b) and c).

functionalization with terminal amine groups to facilitate attachment of negatively charged gold seed nanoparticles formed in a separate process. Synthesis of the silica nanoparticles with both narrow size distribution and rough surface was achieved following a two-phase regrowth procedure. First, uniform silica nanoparticles with 25 nm diameter were synthesized in aqueous phase using a two phase method (**Fig. S1a**).[31] To realize rough surfaced silica particles, 25 nm size silica nanoparticles were regrown into desired size regrowth by the two-phase method (**Fig. S1b**).[32] The gold seeds deposited on the surface of the dielectric cores act as nucleation sites and are allowed to grow in size by further addition of gold precursors.[30]

According to the mechanism and kinetics of gold crystallization,[33, 34] we propose that a balance of kinetic and diffusion rates control the growth of gold nanobranches on a rough silica surface with a peak-valley pattern on which the gold seeds are evenly distributed. (**Fig. 2b and c**). The TEM image in **Fig. 2b** shows the synthesized 80 nm silica nanoparticles with rough surface and uniform size distribution. **Fig. 2c** shows the gold nanoparticle seeds grafted on the rough silica surface-modified with amines. These gold nanoparticles cover the silica nanoparticle surfaces with a discontinuous metal colloid layer (see inset of **Fig. 2c**).

Gold nanobranches were grown from the gold seeds planted on the silica surface under certain conditions, as shown in **Fig. 2d**. The growth of the gold structures depends on the reduction rate and the diffusive mass flux of the gold species to the seeds. If the nucleation rate is much faster that the atom addition, heterogeneous nucleation of gold species occurs in the solution as well as on the attached seeds surfaces[35]. On the other hand, if gold nucleation rate is much slower than the atom addition, kinetic control is achieved and the thermodynamically favoured shape results[36]. For the growth of the gold nanobranches on seeded silica surfaces, pH control of the gold solution precursor solution was required to achieve kinetically controlled conditions.

The gold species grew anisotropically away from the seed to generate gold nanobranches on the surface of the gold seeded silica particles (**Fig. 2d**). We could preferentially grow the seeds located at convex bumps (more accessible) more than at concave bumps (less accessible). Seeds located at the more accessible areas of the roughened silica nanoparticles continuously capture gold species from the reactive solution. Generally, diffusion limitations mean that exposed ends of gold nanobranches tend to grow more rapidly than the perimeter sites with the result of promoting anisotropic growth. Similarly diffusion limitation inhibits the growth of less accessible seeds, contrarily to the case of nanoshell growth[37].

Additionally, polyvinyl pyrrolidone (PVP, 55k), used as a stabilizer, is also reported to promote anisotropic growth of the gold structures in wire-like fashion[38]. Furthermore, the rough surface geometry appears to prevent coalescence of neighbouring gold structures during the growth. On the smooth surface silica particles, distributed gold seeds are equally accessible to the gold species and easily merge with neighbouring gold structures[39]. The formation process for the SGNUs is similar to the mechanism proposed for dendritic nanostructures formation. However, dendritic structures grow as a single crystal structure because the self-aligned attachment mechanism [40, 41].

Addition of base to a $HAuCl_4$ solution hydrolyzes the chloroauric anion in the solution to form six major species with the general form of $[Au(OH)_xCl_{4-x}]^-$, depending on the degree of hydrolysis[42]. Amongst these six gold species, $[Au(OH)_4]^-$ is reported to have the lowest tendency of reduction even with a strong reducing agent[39]. This species becomes dominant at pH ~10.1 during an overnight aging process[43].

Reduction of $[Au(OH)_4]^-$ by ascorbic acid and hydroxylammonium chloride, which are mild reducing agents, inhibits the growth of gold nanobranches, enabling isotropic

growth of gold nanoparticles as shown in **Fig. 3a** (**Fig. S2** and **S3** in the supporting information). Increasing the number of addition cycles of ascorbic acid results in the formation of colloidal gold rather than a gold shell. Ascorbic acid decreases the pH of the solution, promoting the formation of other gold species than $[Au(OH)_4]^-$ [39, 42] that are easily reduced and cause homogeneous nucleation in the solution to form unsupported gold nanoparticles. This observation is supported by an increase of colloidal gold nanoparticles as the number of sequential addition cycles increases. With hydroxylammonium chloride, growth of the gold structures on the silica surfaces becomes limited after the initial stage by diminishing addition to the gold seeds.

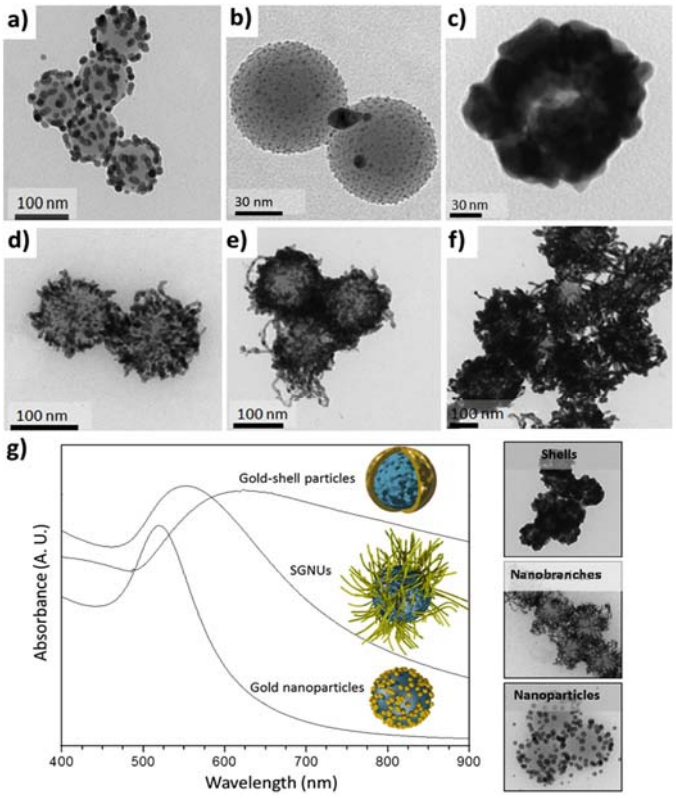

Figure 3. TEM and optical characterization of silica-gold nanostructures synthesized under different conditions. a) TEM image of raspberry-like structures: silica spheres decorated with spherical gold nanoparticles. b) TEM image of gold-seeded silica nanospheres with smooth surface features (see Fig. S1c for smooth silica particles without gold seeds). c) TEM image of silica nanosphere covered with gold shell, with 10 cycles of sequential addition of reducing agent, $NaBH_4$. d-f) TEM images of SGNUs synthesized under ultrasonic agitation with a sequential addition procedure. Sodium borohydride was added as a reducing agent: d) 7 times, e) 15 times and f) 22 times, respectively. g) Optical absorption spectra from silica nanoparticles decorated with different gold structures: shells, gold nanobranches (SGNU) and gold nanoparticles. TEM images on the right correspond to each structure and spectrum.

Growth of gold elongated NPs on the silica nanoparticles is only observed when the gold hydroxide solution is reduced by sodium borohydride, a strong reducing agent. Homogeneous nucleation in the solution is inhibited and a high fraction of gold atoms are deposited over the seeds, as reported by Phonthammachai et al.[39]. The density and length of gold nanobranches increase as the number of cycles of sequential addition goes up; resulting in gold nanobranches as longer as 10 and 100 nm after 7 and 22 reactant addition cycles, respectively (**Fig. S4**).

In order to confirm that the surface topography was a decisive parameter in gold nanobranches growth on the silica surfaces, we explored the synthesis of SGNUs on gold seeded silica particles with same dimensions but having a smooth surface morphology (**Fig. 3b and Fig. S1c**). As expected, based on the proposed mechanism, the gold hydroxide was reduced on the gold seeds that then coalesced to form a complete polycrystalline gold shell around the silica core (**Fig. 3c**).

Addition of reactants in a single step procedure under magnetic stirring was able to grow gold in a linear fashion, but only short gold elongated NPs with uneven diameter were obtained (see **Fig. S5**). On the other hand, ultrasonic radiation promoted a fast gold nanobranches growth even with a single addition (**Fig. S6**). The fast growth in the ultrasonic process can be explained by the fast mass transport from the cavitation induced mixing induced by the ultrasound[44]. A sequential addition of gold solution and reducing agent under ultrasonic radiation was selected as the best method for the synthesis of SGNUs. Under those conditions, deposition of the gold species was controlled by a stable and balanced reduction rate of the $[Au(OH)_4]^-$ during the SGNU formation (**Fig. 3d**). The growth under ultrasonic treatment also implies that the bonding of gold nanobranches to the silica surface is strong enough to withstand acoustic forces on the particles.

Directional growth of the gold nanostructures can be tuned with the number of reactant addition cycles (**Fig. 3d–f**). With 10 cycles of reactant sequential additions, homogenous distribution of gold nanobranches was achieved without crosslinking between themselves. Consequently, kinetic parameters such as mixing, number of reactant addition cycles and reducing agent were key parameters to obtain SGNUs with a controlled morphology of the gold nanobranches. However, sequential addition of reagents was always required to grow the gold nanobranches in controlled manner. This is the most time and cost consuming step in the SGNU synthesis

Fig. 3g shows optical absorbance spectra from different silica-gold nanostructures: core-shells, urchins (SGNUs) and raspberries. The main peak is shifts from 520 nm (raspberries) to over 600 nm (core-shells) with significant enhancement of absorption in near-IR range.

Continuous production of SGNU using microfluidic system

Next we considered the synthesis of SGNU in continuous flow (**Fig. 1b)**. In general, this approach has several advantages over batch processing, including continuous operation, in-line analysis along with control and reproducibility[1, 45]. Moreover, diffusive mixing and mass transfer are enhanced due to the small dimension. Importantly, manipulation of the reagents concentrations in both space and time provides an additional level of reaction control that is not attainable in bulk stirred reactors[46, 47].

Continuous synthesis of SGNU was performed in a flow microreactor made of PTFE tubes and fed by syringe pumps

(**Fig. 1b** and **Fig. S9a** in supporting information). Optimized for highest SGNU quality, the residence time of precursor and reducing agent solution was 12 min. The microreactor showed excellent performance for precise manipulation of reagent concentrations and consequently kinetic control of the reaction during the gold nanobranches crystallization. The flow rate ratio between reducing agent and gold hydroxide solution was adjusted for fine tuning of the $[Au(OH)^4]^-$ reduction rate.

TEM images in **Fig. 4a–d** shows the resulting SGNUs at different flow rate ratios: a) 50:50, b) 20:50 and c) 1:50 ($NaBH_4$:gold precursor solution, in μL/min.). With slower flow rate of $NaBH_4$, the rate of reduction is decreased leading to uniform addition of the gold species to the gold nanobranches. In contrast, higher concentration of $NaBH_4$ facilitates the growth of more active gold nanobranches. As a result, the density of gold nanobranches on the silica surface is reduced while their diameter increases (**Fig. 4a–d**). The diameter of the gold nanobranches falls from 8 nm to 4.5 nm as the $NaBH_4$ concentration decreases from 3.3 mM to 0.13 mM. Optical absorption spectra of SGNUs produced by batch and continuous approaches did not differ significantly (Fig S8). Overall, continuous synthesis of SGNU in a microreactor provided ease of operation with excellent reproducibility, uniformity, morphology control as well as faster reaction rate compared to the batch synthesis. High-resolution TEM images of the SGNU show discontinuous extension of the lattice planes in the gold nanobranches, forming grain boundaries with stacking faults or twins. (**Fig. 4e and f**).

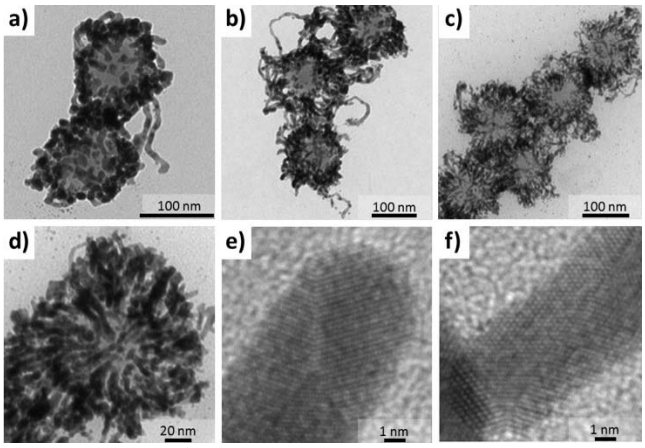

Figure 4. TEM characterization of SGNUs synthesized in flow microreactor system in continuous manner. Residence time in the reactor was 12 min. a–c) Flow rate ratio of $NaBH_4$ solution and gold precursor was varied to control the structure: a) 50:50, b) 20:50 and c) 1:50 ($NaBH_4$:gold precursor solution, μL/min.). d) Magnified TEM image of SGNU at 1:50 ratio (see Fig. S7 for images of other conditions). e) High resolution TEM image showing the tip of a polycrystalline gold nanobranches. f) Root of a gold nanobranch on the silica particle surface.

SERS-active substrate for the evaluation of SGNUs

Metallic structures with sharp edges or tips can significantly enhance the Raman signals by encouraging the surface plasmon resonance,[48] suggesting that the SGNUs with their the densely packed gold nanobranches covering the silica surface could form SERS active substrates. The high aspect ratio of 20−25 (4−5 nm diameter with up to 100 nm length) of gold nanobranches would be expected to lead to enhancement. Based on the localized surface plasmonic resonance of the SGNU presented in Fig. 3g, they would be expected to be responsive over a broad wavelength range, with the strongest resonance in the near IR range.

Herein, we demonstrated the SERS activity of the SGNUs using Rhodamine 6G (R6G, Sigma-Aldrich) as a probe molecule, and 785 nm diode laser as a light source. For the preparation of the SERS substrate from the SGNUs, we have applied two different routes to assemble the nanourchins: 2D planar and 3D spherical shape (**Fig 5a** and **b**).

To make 2D planar SGNU coated substrates, we cast an aqueous suspension of SGNU on to the silicon wafer as shown in **Fig 5a**. This procedure is commonly used and accepted in fabrication of SERS substrates from nanoparticles or nanorods. However, we found that SERS from 2D planer samples made in this way showed some fluctuations from the inhomogeneous distribution of the nanoparticles as well as the applied probe chemicals. Since the substrate preparation step and chemical doping step are separated in this procedure, it is hard to achieve a uniform distribution throughout the whole substrate.

We propose 3D SGNU assemblies as nanoparticle-based SERS substrate with improved distribution of the analyte, as schematically presented in **Fig. 5b**. In this case, we used nanoliter scale aqueous emulsion as a template for the 3D spherical assemblies. Aqueous droplets containing the SGNUs were continuously produced by the glass capillary devices[21]. The produced droplets were collected in the dish filled with non-volatile oil phase. The SGNU droplets then condensed into the 3D spherical aggregates while the water in the droplets slowly evaporated with gentle heating. During drying, the droplets 500 μm diameter shrunk to ~50 μm spherical aggregates. At this size, the SGNU system is able to handle less than 50 nL of sample volumes for SERS data. The 3D substrates yielded more reproducible signals than 2D case since it utilized pre-mixed SGNUs particles with R6G molecules. However, because of its 3D geometry, the signal intensity was affected by the focal point. Besides, when using temperature sensitive chemicals, long evaporation times at elevated temperature could lead to deterioration.

The performance of the prepared SERS-active substrates was characterized with a holographic grating based Raman spectrometer mounted on the microscope with 785 nm diode pumped laser as a light source. As shown in **Fig. 5c**, SERS of 2D substrates from different R6G concentrations show significant enhancement compared with the reference Raman spectra from the bare silica particles without gold urchin structures. When we consider the spot size of the laser (~10 μM with 50X objective lens), the amount of the R6G molecules from the characterizing area was 20.4 pM (~42.6 fg).

Unlike bulk Raman spectra, SERS depend on the material, structure, morphology of the substrates, molecular conformation of the chemicals with the substrate as well as the wavelength of light source. Accordingly, SERS can differ from bulk Raman spectra not only in different intensity ratio between peaks but also in peak locations. Enhancement factors (EF) of 10^7 (at 1605 cm^{-1}) and 10^4 (at 1311 cm^{-1}) were achieved in comparison to bare silica nanoparticles without the gold nanostructures, both doped with R6G (See **Fig. S10a**).

Additionally, SERS spectra with different characteristics are observed from the 2D and 3D substrates as shown in **Fig. 5d**. For example, the peak around 1300 cm^{-1} is strongest from the 3D substrate, whereas peaks around 1600 cm^{-1} are most significant from the 2D substrate. The shape of the spectra from the 3D substrate is more similar to that of bulk R6G Raman spectrum (See **Fig. S10b**). The difference can be interpreted in terms of the distribution or conformation of the R6G molecules during the very different preparation procedures of the 2D and 3D substrates.

For the 2D substrates, the SGNU suspension are dispensed on the silicon wafer, and dried to make planar film. Then, R6G solution is applied on top of the 2D substrate. Therefore, large numbers of the molecules are located near the outer surface of the SGNU substrate, close to the tips of the gold nanobranches. Thus, the interaction between the molecule and the gold nanobranches would be expected to be more dominant.

On the other hand, for the 3D substrates, SGNUs and the R6G molecules are pre-mixed together and aggregated into spherical shape (see **Fig. S10**). Consequently, the R6G molecules are homogeneously distributed throughout the substrate, and there is more chance to be placed in the inner structure, within the gap of neighbouring structures. Preparation time of the 3D substrates is much longer than the 2D substrate, so the SGNUs of the 3D system are more densely packed. (see **Fig. S11**, SEM images of 2D and 3D substrates)

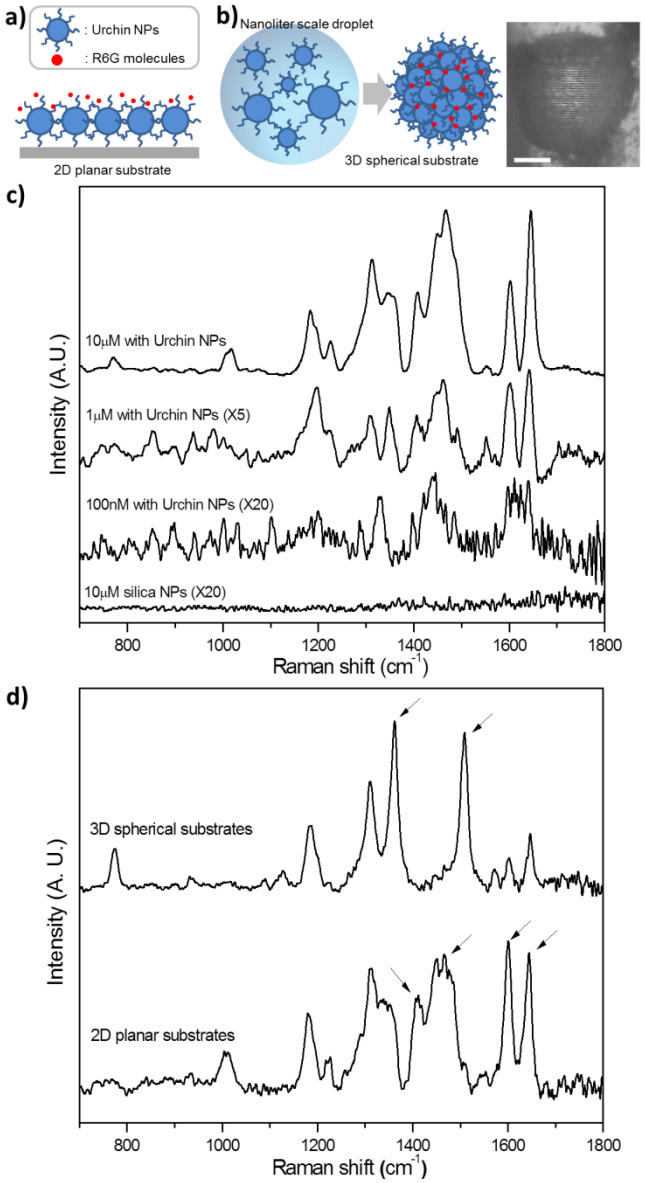

Figure 5. Surface enhance Raman spectra (SERS) of Rhodamine 6G (R6G) on the 2D and 3D SGNU substrates. a, b) Scheme for the preparation of SGNU-based SERS-active substrates in 2D and 3D forms. a) Scheme of 2D planar assembly prepared on the silicon wafer by drop-casting of SGNU suspension. R6G solutions were then applied for SERS characterization after the casting. b) Scheme of 3D spherical assembly prepared using water in oil emulsion as a template. Emulsions containing premixed R6G solution and SGNU suspension were produced in the microfluidic drop-generator and then casted into spherical assemblies by evaporating water from the emulsion (See Fig. S8). Right figure shows IR image of 3D SGNU assembly taken during SERS measurement. Interference of 785 nm laser beam (white area) can be seen from the scattering on the surface. Scale bar is 5 μm. c) SERS of R6G on 2D SGNU substrates with different concentration range (100 nM–10 μM). d) Comparison between 2D and 3D substrates showing different SERS finger print. Black arrows represent distinctive peaks.

Materials and Methods

Materials

Tetraethylorthosilicate (TEOS, Sigma-Aldrich, 99.999%), NH_3OH (Sigma-Aldrich,28 wt% in water), K_2CO_3 (Aldrich),3-Aminopropyltriethoxysilane (APTES,Sigma-Aldrich), octane (Sigma-Aldrich), L-lysine (Sigma-Aldrich), ethanol (Merck, HPLC grade), cyclohexane (Sigma-Aldrich), $HAuCl_4$ (Aldrich), $NaBH_4$ (Aldrich), Ascorbic Acid (Aldrich), hydroxyl-ammonium chloride (Aldrich) Polyvinyl pyrrolidone (PVP, MW = 55000, Aldrich) and Rhodamine 6G (R6G Aldrich)

Preparation of the silica nanoparticles

Synthesis of uniform silica seed particles. Uniform silica nanoparticles with 25 nm diameter were synthesized in aqueous phase using a two phase method. Unlike conventional sol-gel procedure which is done in the single phase, the two phase method separates the silica precursor tetraethoxyorthosilicate (TEOS) from the water by dissolving the precursor into immiscible organic solvent. Diffusion of the TEOS molecules into the aqueous phase is restricted by limited solubility of the octane and thus prevented from rapid mixing. At such low precursor concentration in the aqueous phase, undesired

nucleation is controlled and uniform particles are formed. L-lysine molecules contribute to accelerate the reaction by forming basic conditions. Additionally, L-lysine served as surfactant reducing the surface energy and confines the reaction in its micelle-like complex to lead to uniform and small silica nanoparticles.

For the experiment, L-lysine (100 mg) powder was first dissolved in distilled water (100 mL) and stirred at 80 °C. Then, mixture of octane (5 mL) and tetraethylorthosilicate (7mL, TEOS) was added to the aqueous solution. The final solution was stirred for 24 h at 80 °C and then quenched in cold water to terminate the reaction. The particles were centrifuged 3 times and washed with distilled water. **Fig S1a** shows TEM image of synthesized 25 nm silica nanoparticles with uniform distribution.

Synthesis of rough surfaced silica

In order to grow rough surfaced silica particles of 80 nm diameter, the 25 nm size uniform silica nanoparticles served as seeds for the regrowth. We again performed two phase synthesis with 10 mL of the seed solution. This solution was combined with 90 mL distilled water and 14 mg L-lysine and then stirred at 90 °C. The accelerated diffusion rate at high temperature led to a rough surface morphology of the silica particles. Subsequently, a mixture of octane and TEOS was added to the solution. The reagent used for the reaction was 1 mL of as-prepared silica seeds (silica concentration of 0.315 M), 3.6 mL of water, 0.5 mL of cyclohexane, and 0.352 mL of TEOS. The final solution was stirred for 30 h at 90 °C. The particles were centrifuged 3 times and washed with distilled water. **Fig S1b** shows a TEM image of the synthesized 80 nm silica nanoparticles with rough surface and uniform size distribution.[32]

Synthesis of smooth surfaced silica

For the smooth surfaced silica nanoparticles, silica seeds were grown by conventional Stöber procedure. First, silica seeds dispersed in the aqueous phase were mixed with ethanol and ammonium hydroxide. TEOS was added for 4 h using a syringe pump (Harvard, PHD Ultra). For the final size of 80 nm, 1 mL of as-prepared silica seeds (silica concentration of 0.315 M), 3.6 mL of water, 0.5 mL of cyclohexane, and 0.352 mL of TEOS were used for the reaction. The particles were centrifuged 3 times and washed with distilled water. The TEM image in Error! Reference source not found. **S1c** shows the synthesized 80 nm silica nanoparticles with smooth surface and uniform size distribution.

APTES-Grafted Silica nanoparticles.

Silica particles were re-dispersed in ethanol with a mass ratio of 4:1 (ethanol: silica particles). Surfaces of the silica NPs were then functionalized with 10 mM aminopropyl triethoxysilane (APTES) under stirring at 80 ºC for 3 h. After being cooled to room temperature, the amine grafted silica nanoparticles were then centrifuged at 9000 rpm for 10 min and washed with absolute ethanol for four cycles. Finally the particles were re-suspended in Milli-Q water.

Gold seeding on the surface of the silica noanoparticles

Gold seeds of 2–3 nm size were prepared according to the method reported by Duff et al.[49]. The grafting of an amine terminated silane coupling agent (APTES) to the silica surface enables the bonding with the colloidal gold particles[30].

Preparation of the SGNUs

60 mg of K_2CO_3 was added to 1.5 mL of 25 mM $HAuCl_4$ diluted in 100 mL of water and allowing the solution to stir in the dark overnight at room temperature for the $HAuCl_4$ to hydrolyze and age to give a colorless gold hydroxide solution. pH was measured to be 10.1. A reducing agent solution of 6.3 mM $NaBH_4$, Ascorbic Acid and hydroxylammonium chloride) was prepared. $NaBH_4$ solution was kept in an ice bath. A Polyvinyl pyrrolidone (PVP, MW = 55000) solution was used as a stabilizing agent, 3 mg/mL (PVP/solution). Ultrasound radiation and magnetic stirring was used in the SGNU growth experiments.

SINGLE ADDITION PROCEDURE

190 μL of Au-seeded silica nanoparticles were added to 10 mL of gold hydroxide solution. 1 mL of PVP solution was vigorously stirred with previous solution and 1 mL of reducing agent $NaBH_4$ was added. After reaction was completed, the SGNU particles were centrifuged and redispersed in distilled water.

SEQUENTIAL ADDITION PROCEDURE

190 μL of Au-seeded silica nanoparticles were added to 1 mL of gold hydroxide solution. 1 mL of PVP solution was vigorously stirred with previous solution and 100 μL of reducing agent was added. 1 mL Gold hydroxide solution and 100 μL of reducing agent were added sequentially every 2 minutes (**Fig 1a**). After reaction was completed, the SGNU particles were centrifuged and redispersed in distilled water.

CONTINUOUS PRODUCTION OF SGNU IN A MICROFLUIDIC REACTOR

A 10 mL plastic syringe was filled with a solution constituted by 190 μL of Au-seeded silica nanoparticles, 10 mL of gold hydroxide solution and 1 mL of PVP solution. Reducing agent, $NaBH_4$, was filled in a 5 mL plastic syringe and was kept cold using ice. A Teflon tubing reactor was immersed in an ultrasound bath and solutions filling both syringes were pumped by two syringe pumps (Harvard) at different flow rates. The PTFE tubing used in these experiments had 1/16" outer diameter and 800μm inner diameter. The length of the tubing was adjusted to realize the desired residence time. Gold solution was injected at 50 μL/min and reducing agent flow rate was varied from 50 to 1 μL/min, respectively (**Fig 1b**). After

solution was collected at the outlet, the SGNU particles were centrifuged and redispersed in distilled water.

Preparation of the 2D planar SGNU substrates

To make two-dimensional (2D) planar SGNU structures, we cast 5 μL of aqueous SGNU suspension on the silicon wafer. Prior to the casting, the silicon wafer was treated with oxygen plasma to enhance the wetting of aqueous solution and ensure the formation of a uniform liquid film. Then, the SGNU particles were cast as 2D planar substrates after drying at room temperature for 10 min. 5 μL of Raman-active R6G solution with different concentrations (100 nM−10 μM of R6G in milli-Q water) were applied to the substrate. The background Raman spectrum of the crystalline silicon (521 cm^{-1}) did not obstruct the spectrum coming from the R6G over the range of interest.

Preparation of the 3D spherical SGNU substrates

An aqueous mixture of SGNU particles and R6G (10 μM) was injected through the inner nozzle of the concentric glass capillary device, while an immiscible oil phase (hexadecane, Sigma-Aldrich) flowed from the outer capillary. The resulting Rayleigh instability caused the aqueous phase to break into a train of emulsion droplets. The hexadecane phase contained 0.5 wt% of surfactants (ABIL EM90, Evonik) to prevent coalescence. Flow rates were 20 μL/min for the inner aqueous phase and 60 μL/min for the outer oil phase. The generated emulsions were then collected on a Teflon dish and evaporated at 70 °C for 24 hr to remove water selectively from the aqueous phase. The hexadecane phase was non-volatile at this temperature. The confinement by each single droplet shaped the assembly of SGNU nanoparticles during the drying process.

SERS measurements

A holographic grating based spectrograph with fiber-coupled microscope (Kaiser Optical System, Hololab 5000R) was used obtain SERS spectra from the SGNU structures,. The light source was a 785 nm diode pumped laser (Kaiser Optical System, Invictus, CW, variable output power10−400mW). All the measurements were performed with 7 mW/cm^2 output power, and 1 to 60 s of integration time without accumulation.

Conclusions

A new method based on the combination of molecular self-assembly and reduction chemistry of gold species has been exploited to achieve growth of SERS-active gold nanobranches via a fast and reproducible procedure on the surface of silica nanoparticles. The surface roughness of the silica nanoparticle substrates together with kinetic parameters and reagent addition were determining factors in promoting urchin-like growth of the gold structures. Continuous microfluidic synthesis of the SGNUs provided better control and reproducibility through manipulation of the reagent ratio and enhanced mixing. The synthesized SGNUs exhibited significant enhancement of SERS signals from their unique urchin-like morphology with abundant sharp tips.

Acknowledgements

Authors acknowledge US NSF grant (CHE-0714189) for funding this research. V.S. acknowledges the support of the Fulbright Commission and the Ministry of Education in Spain (Programa Nacional de Movilidad de RR.HH. del Plan Nacional de I+D+I 2008- 2011)

Notes and references

[a] Department of Chemical Engineering. Massachusetts Institute of Technology, 77 Massachusetts Avenue, Cambridge, MA 02139, United States

*E-mail: kfjensen@mit.edu

‡ These authors contributed equally.

Present addresses:

[b] Department of Chemical Engineering, Instituto de Nanociencia de Aragon, Universidad Zaragoza C/Pedro Cerbuna 12, 50009 Zaragoza (Spain)

[c] Radioisotope Research Division. Korea Atomic Energy Research Institute, 989-111 Daedeok-daero, Yuseong-gu, Daejeon, 305-353, Republic of Korea

Electronic Supplementary Information (ESI) available: [details of any supplementary information available should be included here]. See DOI: 10.1039/b000000x/

1. S. Marre and K. F. Jensen, *Chemical Society Reviews*, 2010, 39, 1183-1202.
2. V. Sebastian, M. Arruebo and J. Santamaria, *Small*, 2014, 10, 835–853.
3. J. Baek, P. M. Allen, M. G. Bawendi and K. F. Jensen, *Angewandte Chemie-International Edition*, 2011, 50, 627-630.
4. J. X. Fang, S. Y. Du, S. Lebedkin, Z. Y. Li, R. Kruk, M. Kappes and H. Hahn, *Nano Letters*, 2010, 10, 5006-5013.
5. V. Sebastian, S. K. Lee, C. Zhou, M. F. Kraus, J. G. Fujimoto and K. F. Jensen, *Chem Commun*, 2012, 48, 6654-6656.
6. S. K. Lee, X. Y. Liu, V. S. Cabeza and K. F. Jensen, *Lab Chip*, 2012, 12, 4080-4084.
7. S. M. Nie and S. R. Emery, *Science*, 1997, 275, 1102-1106.
8. J. P. Camden, J. A. Dieringer, J. Zhao and R. P. Van Duyne, *Accounts of Chemical Research*, 2008, 41, 1653-1661.
9. Y. W. C. Cao, R. C. Jin and C. A. Mirkin, *Science*, 2002, 297, 1536-1540.
10. P. K. Jain, X. H. Huang, I. H. El-Sayed and M. A. El-Sayed, *Accounts of Chemical Research*, 2008, 41, 1578-1586.
11. J. B. Jackson and N. J. Halas, *Proceedings of the National Academy of Sciences of the United States of America*, 2004, 101, 17930-17935.
12. J. N. Anker, W. P. Hall, O. Lyandres, N. C. Shah, J. Zhao and R. P. Van Duyne, *Nature Materials*, 2008, 7, 442-453.
13. E. J. Smythe, M. D. Dickey, J. M. Bao, G. M. Whitesides and F. Capasso, *Nano Letters*, 2009, 9, 1132-1138.
14. X. Y. Zhang, E. M. Hicks, J. Zhao, G. C. Schatz and R. P. Van Duyne, *Nano Letters*, 2005, 5, 1503-1507.

15. J. F. Li, Y. F. Huang, Y. Ding, Z. L. Yang, S. B. Li, X. S. Zhou, F. R. Fan, W. Zhang, Z. Y. Zhou, D. Y. Wu, B. Ren, Z. L. Wang and Z. Q. Tian, *Nature*, 2010, 464, 392-395.
16. C. L. Haynes, A. D. McFarland and R. P. Van Duyne, *Analytical Chemistry*, 2005, 77, 338a-346a.
17. M. I. Stockman, S. V. Faleev and D. J. Bergman, *Physical Review Letters*, 2001, 87, art. no.-167401.
18. S. H. Sun, C. B. Murray, D. Weller, L. Folks and A. Moser, *Science*, 2000, 287, 1989-1992.
19. S. H. Chen, Z. L. Wang, J. Ballato, S. H. Foulger and D. L. Carroll, *Journal of the American Chemical Society*, 2003, 125, 16186-16187.
20. H. J. You, Y. T. Ji, L. Wang, S. C. Yang, Z. M. Yang, J. X. Fang, X. P. Song and B. J. Ding, *J Mater Chem*, 2012, 22, 1998-2006.
21. X. S. Wang, D. P. Yang, P. Huang, M. Li, C. Li, D. Chen and D. X. Cui, *Nanoscale*, 2012, 4, 7766-7772.
22. Y. J. Ye, J. Chen, Q. Q. Ding, D. Y. Lin, R. L. Dong, L. B. Yang and J. H. Liu, *Nanoscale*, 2013, 5, 5887-5895.
23. C. J. Orendorff, L. Gearheart, N. R. Jana and C. J. Murphy, *Physical Chemistry Chemical Physics*, 2006, 8, 165-170.
24. A. G. Brolo, E. Arctander, R. Gordon, B. Leathem and K. L. Kavanagh, *Nano Letters*, 2004, 4, 2015-2018.
25. D. H. Jeong, Y. X. Zhang and M. Moskovits, *Journal of Physical Chemistry B*, 2004, 108, 12724-12728.
26. N. Zettsu, J. M. McLellan, B. Wiley, Y. D. Yin, Z. Y. Li and Y. N. Xia, *Angewandte Chemie-International Edition*, 2006, 45, 1288-1292.
27. J. T. Zhang, X. L. Li, X. M. Sun and Y. D. Li, *Journal of Physical Chemistry B*, 2005, 109, 12544-12548.
28. O. M. Bakr, B. H. Wunsch and F. Stellacci, *Chem Mater*, 2006, 18, 3297-3301.
29. B. Plowman, S. J. Ippolito, V. Bansal, Y. M. Sabri, A. P. O'Mullane and S. K. Bhargava, *Chem Commun*, 2009, 5039-5041.
30. S. J. Oldenburg, R. D. Averitt, S. L. Westcott and N. J. Halas, *Chemical Physics Letters*, 1998, 288, 243-247.
31. T. Yokoi, Y. Sakamoto, O. Terasaki, Y. Kubota, T. Okubo and T. Tatsumi, *Journal of the American Chemical Society*, 2006, 128, 13664-13665.
32. K. D. Hartlen, A. P. T. Athanasopoulos and V. Kitaev, *Langmuir*, 2008, 24, 1714-1720.
33. J. Polte, T. T. Ahner, F. Delissen, S. Sokolov, F. Emmerling, A. F. Thunemann and R. Kraehnert, *Journal of the American Chemical Society*, 2010, 132, 1296-1301.
34. B. K. Pong, H. I. Elim, J. X. Chong, W. Ji, B. L. Trout and J. Y. Lee, *Journal of Physical Chemistry C*, 2007, 111, 6281-6287.
35. M. R. Rasch, K. V. Sokolov and B. A. Korgel, *Langmuir*, 2009, 25, 11777-11785.
36. N. R. Jana, L. Gearheart and C. J. Murphy, *Journal of Physical Chemistry B*, 2001, 105, 4065-4067.
37. T. A. Witten and L. M. Sander, *Physical Review Letters*, 1981, 47, 1400-1403.
38. D. S. Guo, Wen, S. Dong, E. Wang, *Talanta*, 2009, 77, 1510-1517.
39. N. Phonthammachai, J. C. Y. Kah, G. Jun, C. J. R. Sheppard, M. C. Olivo, S. G. Mhaisalkar and T. J. White, *Langmuir*, 2008, 24, 5109-5112.
40. J. X. Fang, X. N. Ma, H. H. Cai, X. P. Song and B. J. Ding, *Nanotechnology*, 2006, 17, 5841-5845.
41. T. Qiu, X. L. Wu, G. G. Siu and P. K. Chu, *Applied Physics Letters*, 2005, 87.
42. C. K. Chang, Y. J. Chen and C. T. Yeh, *Applied Catalysis a-General*, 1998, 174, 13-23.
43. F. Moreau, G. C. Bond and A. O. Taylor, *Journal of Catalysis*, 2005, 231, 105-114.
44. K. S. Suslick and G. J. Price, *Annual Review of Materials Science*, 1999, 29, 295-326.
45. B. K. H. Yen, N. E. Stott, K. F. Jensen and M. G. Bawendi, *Advanced Materials*, 2003, 15, 1858-1862.
46. V. S. Cabeza, S. Kuhn, A. A. Kulkarni and K. F. Jensen, *Langmuir*, 2012, 28, 7007-7013.
47. L. Gomez, M. Arruebo, V. Sebastian, L. Gutierrez and J. Santamaria, *J Mater Chem*, 2012, 22, 21420-21425.
48. E. Bailo and V. Deckert, *Chemical Society Reviews*, 2008, 37, 921-930.
49. D. G. Duff, A. Baiker and P. P. Edwards, *Langmuir*, 1993, 9, 2301-2309.

ARTICLE

SYNOPSIS TOC

Engineering the synthesis of silica-gold nano-urchin particles using continuous synthesis

Victor Sebastian, Seung-Kon Lee and Klavs F. Jensen